Journal of Volcanology and Geothermal Research 256 (2013) 87–95

Contents lists available at SciVerse ScienceDirect

Journal of Volcanology and Geothermal Research

journal homepage: www.elsevier.com/locate/jvolgeores

Pre-eruption deformation caused by dike intrusion beneath Kizimen volcano, Kamchatka, Russia, observed by InSAR

Lingyun Ji [a], Zhong Lu [b,*], Daniel Dzurisin [b], Sergey Senyukov [c]

[a] Second Crust Monitoring and Application Center, China Earthquake Administration, Xi'an, Shaanxi, China
[b] Cascades Volcano Observatory, U.S. Geological Survey, Vancouver, WA, USA
[c] Kamchatkan Branch of Geophysical Survey, Russia Academy of Sciences, Petropavlovsk-Kamchatsky, Russia

ARTICLE INFO

Article history:
Received 21 July 2012
Accepted 15 February 2013
Available online 27 February 2013

Keywords:
Interferometric synthetic aperture radar
InSAR
Radar
Geodesy
Kizimen
Diking

ABSTRACT

Interferometric synthetic aperture radar (InSAR) images reveal a pre-eruption deformation signal at Kizimen volcano, Kamchatka, Russia, where an ongoing eruption began in mid-November, 2010. The previous eruption of this basaltic andesite-to-dacite stratovolcano occurred in 1927–1928. InSAR images from both ascending and descending orbital passes of Envisat and ALOS PALSAR satellites show as much as 6 cm of line-of-sight shortening from September 2008 to September 2010 in a broad area centered at Kizimen. About 20 cm of opening of a nearly vertical dike provides an adequate fit to the surface deformation pattern. The model dike is approximately 14 km long, 10 km high, centered 13 km beneath Kizimen, and strikes NE–SW. Time-series analysis of multi-temporal interferograms indicates that (1) intrusion started sometime between late 2008 and July 2009, (2) continued at a nearly constant rate, and (3) resulted in a volume expansion of 3.2×10^7 m^3 by September 2010, i.e., about two months before the onset of the 2010 eruption. Earthquakes located above the tip of the dike accompanied the intrusion. Eventually, magma pressure in the dike exceeded the confining strength of the host rock, triggering the 2010 eruption. Our results provide insight into the intrusion process that preceded an explosive eruption at a Pacific Rim stratovolcano following nearly a century of quiescence, and therefore have implications for monitoring and hazards assessment at similar volcanoes elsewhere.

Published by Elsevier B.V.

1. Introduction

The Kamchatka volcanic arc is located along the northwestern Pacific Rim, which comprises two main segments: the Sredinny Range (SR) in the west and East Kamchatka Range in the east (Kozhurin, 2004; Ponomareva et al., 2007) (Fig. 1). The East Kamchatka Range is subdivided further into the Eastern Volcanic Front (EVF) and the Central Kamchatka Depression (CKD) volcanic zone (Ponomareva et al., 2007). Kizimen volcano, one of the active volcanoes in the East Kamchatka Range, is located at the boundary between CKD and EVF (Fig. 1). The area around Kizimen is cut by a complex system of NE–SW-trending, westward-dipping normal faults (Melekestsev et al., 1995; Browne et al., 2010).

The Kizimen edifice started growing in Late Pleistocene time, about 11–12 thousand years ago (Melekestsev et al., 1995). Several catastrophic eruptions occurred during the evolution of Kizimen (Melekestsev et al., 1995). An explosive eruption about 1100 years ago produced a lateral blast and created a crater breached to the northeast. All eruptive products from Kizimen are mid-potassic basaltic andesite-to-dacite of the calcalkaline series (Melekestsev et al., 1995). Prior to 2010, only a single explosive eruption in 1927–1928 had occurred during historical time (Siebert and Simkin, 2002).

The latest eruption at Kizimen volcano began around mid-November of 2010, and finished on December 9th 2012 (VONA/KVERT, 2012). The eruption was preceded by strong and long-lasting increased seismicity starting in April 2009 (Senyukov et al., 2011). The early phase of the eruption was characterized by increased fumarolic activity on October 16 and episodic ash emission on November 11, 2010 (Senyukov et al., 2011). According to seismic data (Senyukov et al., 2011) and satellite observations (Melnikov et al., 2011), explosive events occurred on December 12 and 31, 2010, January 6, 12 and 15, March 7 and May 2, 2011. The first explosive eruption lasted approximately 20 min and lofted an ash plume to an altitude of ~10 km, which drifted to the northwest. The March and May 2011 events produced not only vertical eruption columns but also large pyroclastic flows. An elevated level of local seismicity has characterized the entire eruption sequence.

Many volcanic eruptions are preceded by a period of surface inflation (i.e., uplift and tumescence) caused by an increase in subsurface volume and/or a pressure increase in a magma reservoir beneath the volcano (e.g. Dvorak and Dzurisin, 1997; Dzurisin, 2007). Therefore, surface deformation measurements are important for understanding volcanic processes and hazards, and they can provide important insights into the structure, plumbing, and state of restless volcanoes.

* Corresponding author. Tel.: +1 36 993 8911; fax: +1 36 9938981.
E-mail address: lu@usgs.gov (Z. Lu).

0377-0273/$ – see front matter. Published by Elsevier B.V.
http://dx.doi.org/10.1016/j.jvolgeores.2013.02.011

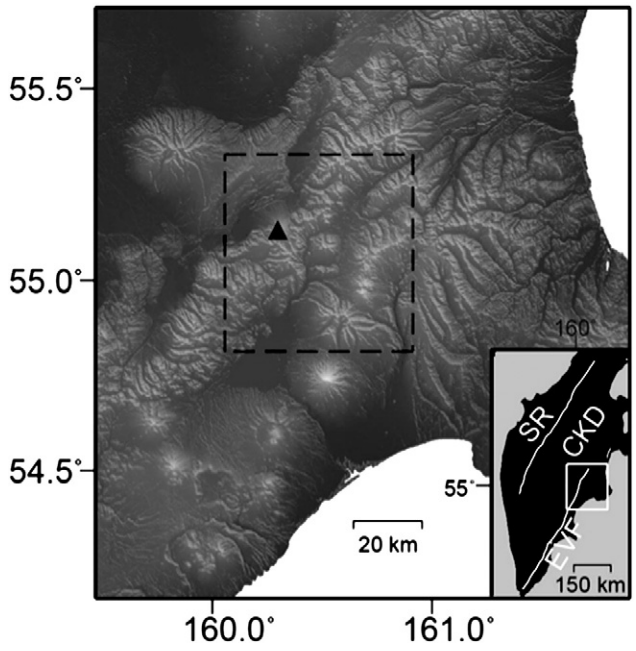

Fig. 1. Shaded relief map of Kizimen volcano and vicinity. Black triangle marks the location of Kizimen. Dashed box marks the area covered by interferograms shown in Figs. 2–4. Inset shows the location of Kizimen at the border between the Central Kamchatka Depression (CKD) and Eastern Volcanic Front (EVF), both in Kamchatka, Russia. White lines represent the EVF and Sredinny Range (SR) volcanic belts.

Table 1
Line-of-sight (LOS) vectors for 6 satellite tracks used in this study.

Track	LOS Vector (East, North, Up)
358	(−0.616 −0.114 0.780)
123	(−0.377 −0.091 0.922)
352	(−0.345 −0.084 0.935)
395	(−0.408 −0.099 0.908)
059	(0.377 −0.091 0.922)
288	(0.346 −0.083 0.935)

There is no ground-based deformation monitoring network on Kizimen volcano due to its remoteness, persistently inclement weather, and difficult logistics. This makes the application of satellite-based monitoring techniques such as interferometric synthetic aperture radar (InSAR) highly desirable. InSAR combines two or more SAR images of the same area acquired at different times from nearly the same vantage point in space to map any surface deformation that might occur during the time interval spanned by the images (e.g., Massonnet and Feigl, 1998; Rosen et al., 2000). InSAR has been demonstrated to be an important tool for investigating volcanic deformation and understanding magma supply dynamics at many of the world's volcanoes (e.g., Massonnet et al., 1995; Amelung et al., 2000; Lu et al., 2000; Pritchard and Simons, 2004; Lu et al., 2005; Wright et al., 2006; Yun et al., 2006; Lu, 2007; Calais et al., 2008; Biggs et al., 2010; Lu et al., 2010).

At Kamchatkan volcanoes, Lundgren and Lu (2006) successfully detected an episodic magma intrusion event during 2000–2003 at Uzon caldera using Envisat and Radarsat-1 images. No significant deformation was observed at several Kamchatkan volcanoes that erupt frequently, including Kliuchevskoi, Sheveluch, and Bezymianny (Pritchard and Simons, 2004; Lundgren and Lu, 2006). Here we present InSAR observations of pre-eruption deformation at Kizimen volcano. More than 6 cm of surface displacement in the satellite's line-of-sight (LOS) direction is mapped from multi-temporal InSAR images acquired from 2008 to 2010. Our preferred explanation is that a magma-filled dike intruded beneath volcano, causing a broad pattern of surface deformation and eventually triggering the eruption that began in mid-November 2010.

2. InSAR data and analysis

To achieve the best coherent interferograms for Kizimen volcano, we only chose SAR images acquired during the summer and early fall (from mid-June to mid-October) to avoid coherence loss due to snow and ice. SAR images used for this study were acquired from two sensors (Envisat and ALOS satellites) operating at two different wavelengths (C-band and L-band, respectively), with a total of 6 different viewing geometries (Table 1). We used the two-pass InSAR approach (e.g. Massonnet and Feigl, 1998; Rosen et al., 2000) to form 14 deformation interferograms with good coherence (Table 2). A digital elevation model (DEM) from the Shuttle Radar Topography Mission (SRTM) (Farr et al., 2007) with 90 m pixel spacing was used to remove the topographic signature from the InSAR phase maps. To remove residual orbit errors, a fine estimation of the interferogram baseline was obtained by nonlinear least-square adjustment of the observed phase over presumably stable areas (Rosen et al., 1996; Lu, 2007) (Table 2). For the interferograms that are obviously contaminated by topography-correlated atmospheric delays, we made a linear correction based on topographic height, using phase observations of areas far from the volcano as a guide (Table 2).

Fig. 2 shows examples of Kizimen interferograms that span time intervals of several months to a few years. Together these interferograms map patterns of deformation from 2004 to September 2010, i.e., about 2 months before the start of the eruption, and lead to the following observations:

Table 2
SAR images used for this study.

Master date	Slave date	Satellite/track ID	Orbit mode	Bn (m)	Baseline refinement	Atmospheric correction
20040730	20070824	E059	D	61	No	No
20070725	20100917	A358	A	1785	No	No
20070805	20090809	E288	D	10	Yes	Yes
20070805	20100829	E288	D	56	Yes	Yes
20070824	20080704	E059	D	−107	No	No
20070909	20100802	A358	A	1350	Yes	No
20080808	20090828	E059	D	54	No	Yes
20080808	20100917	E059	D	75	No	Yes
20080917	20100714	E123	A	37	No	Yes
20090809	20100829	E288	D	46	No	No
20090814	20100903	E352	A	25	No	Yes
20090817	20100906	E395	A	75	No	Yes
20090828	20100917	E059	D	21	No	Yes
20100802	20100917	A358	A	135	Yes	No

Note: Dates are image acquisition times in yyyymmdd format (read 20040730 as 30 July 2004). Also included are satellite ID (E is Envisat and A is ALOS), track ID (059, 123, 288, 352, 358, 395), orbit mode (A is Ascending and D is Descending). Bn is the perpendicular baseline of the corresponding InSAR pair. For each InSAR pair, baseline refinement or topography-related atmospheric correction is indicated.

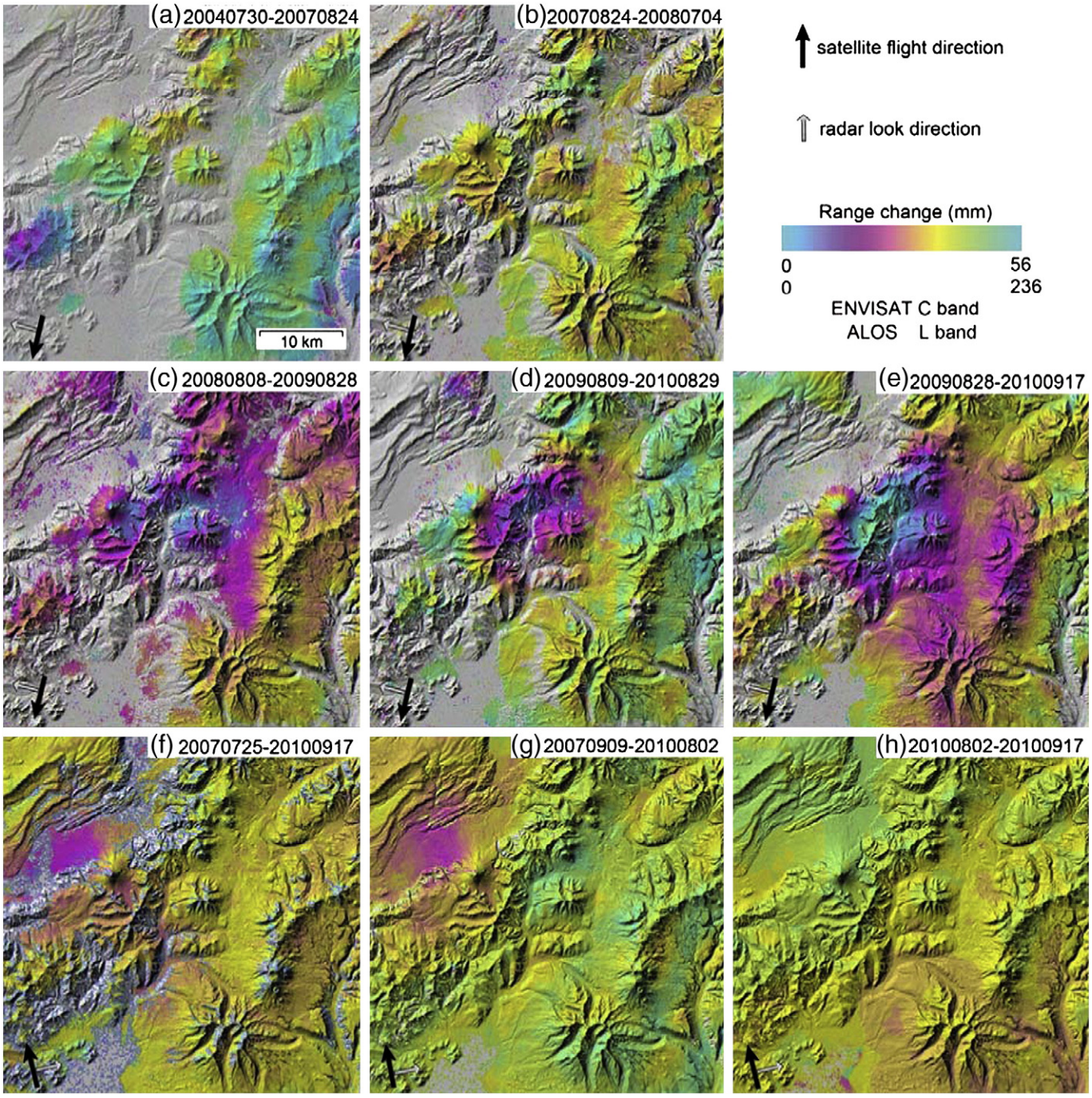

Fig. 2. Kizimen interferograms spanning the following periods (date format is yyyymmdd): (a) 20040730–20070824 (ENVISAT Track 059), (b) 20070824–20080704 (ENVISAT Track 059), (c) 20080808–20090828 (ENVISAT Track 059), (d) 20090809–20100829 (ENVISAT Track 288), (e) 20090828–20100917 (ENVISAT Track 059), (f) 20070725–20100917 (ALOS PALSAR Path 358), (g) 20070909–20100802 (ALOS PALSAR Path 358) and (g) 20100802–20100917 (ALOS PALSAR Path 358). Satellite flight direction and radar look direction are labeled. Each fringe (full color cycle) represents 56 mm or 236 mm of range change between the ground and satellite for ENVISAT (a–e) and ALOS (f–h), respectively. Areas that lack interferometric coherence are uncolored.

1. Interferometric coherence is better at L-band than at C-band. More specifically, the coherence in Fig. 2, interferograms f–h, is considerably higher than that of any others. In all C-band interferograms, coherence in the area immediately northwest of Kizimen is lost after a few months due to dense vegetation. In addition, coherence elsewhere in the study area decreases considerably with time.
2. Although a correction was applied to the interferograms in an attempt to remove topography-correlated atmospheric artifacts, these seem to persist in some cases. For example, fringes in the southeastern part of Fig. 2a and e correlate with topography and have the appearance of atmospheric artifacts. On the other hand, large-scale fringes centered at Kizimen that persist in time (e.g. Fig. 2d–g) are unlikely to be atmospheric artifacts, because these interferograms were produced from independent SAR images acquired on different dates. Also, the Kizimen signal cannot be attributed to DEM error because the baselines of these interferograms are short, making them insensitive to any plausible errors in the DEM.
3. The interferograms show no ground deformation near Kizimen during 2004–08 (Fig. 2a, b), but from September 2008 to September 2010 a persistent pattern of deformation is apparent in several interferograms from different sensors and tracks (Fig. 2c–g). In C-band interferograms from descending tracks (Fig. 2c–e), maximum line-of-sight (LOS)

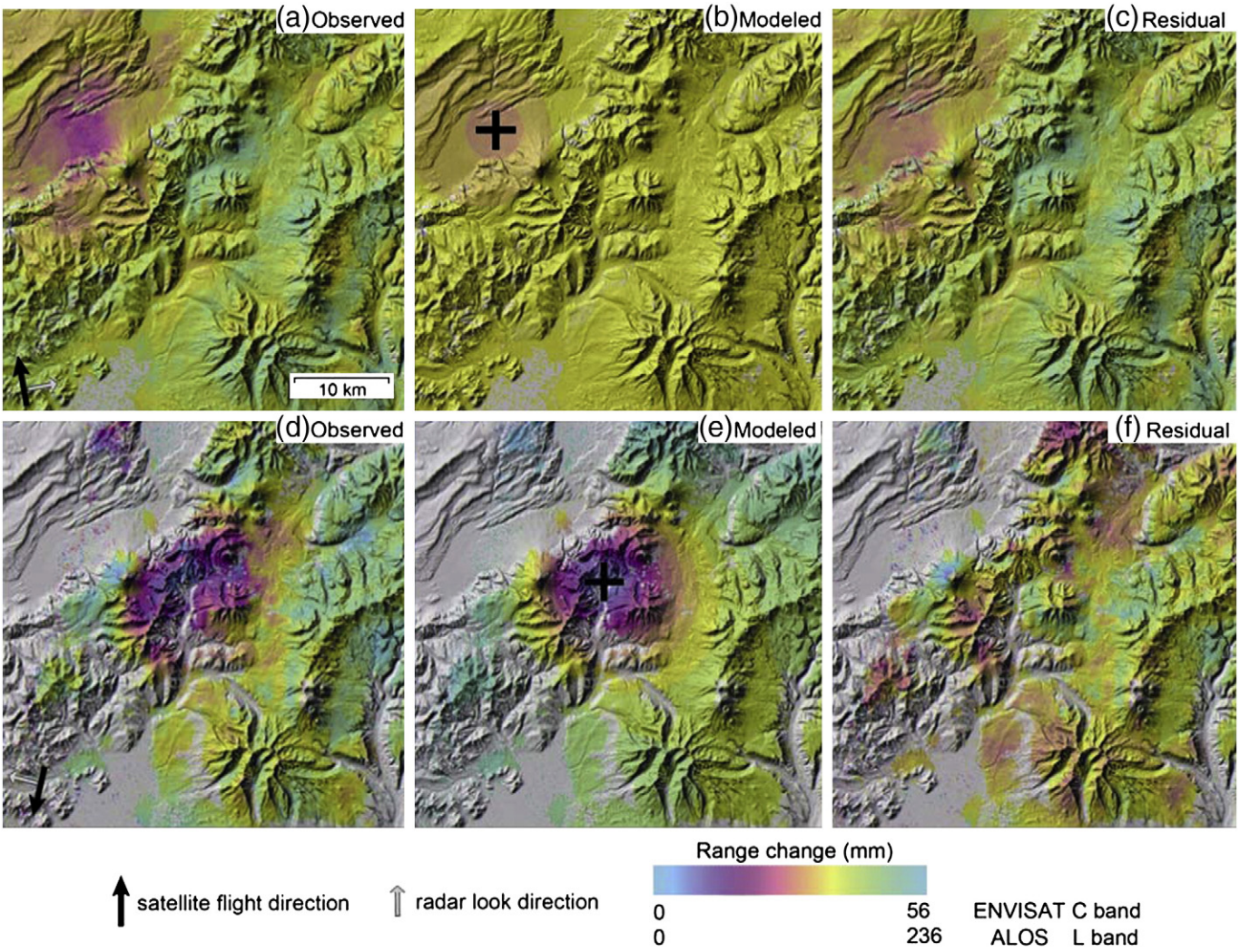

Fig. 3. (Left) Observed interferograms with the best coherence spanning (a) 20070909–20100802 (ALOS PALSAR Path 358) and (d) 20090809–20100829 (ENVISAT Track 288); (middle) (b, e) synthetic interferograms for Mogi sources that best fit the individual interferograms; (right) (c, f) residual interferograms, which are the differences between observed (left) and modeled (middle) interferograms. Black crosses in (b) and (e) represent the surface positions of the corresponding best-fit Mogi sources. Satellite flight direction and radar look direction are labeled on the observed interferograms. Each fringe (full color cycle) represents 56 mm or 236 mm of range change between the ground and the satellite for ENVISAT (Figures a–c) and ALOS (d–f), respectively. Areas that lack interferometric coherence are uncolored.

shortening of about 6 cm occurred in an area about 15 km in diameter centered east of Kizimen. L-band interferograms from ascending tracks show maximum LOS shortening of about 4 cm in an area about 10 km in diameter centered west of Kizimen (Fig. 2f, g), where the C-band interferograms do not maintain coherence.

4. The observed deformation occurred progressively from September 2008 to September 2010, not suddenly or over a period of less than a few months. No useful Envisat or ALOS PALSAR images suitable for InSAR processing were acquired after September 17, 2010, about 2 months before the start of the 2010 eruption. The final pre-eruption interferogram, which spans 46 days from August 2 to September 17, 2010 (Fig. 2h), does not show accelerated deformation relative to the others, so we suspect that the deformation occurred at a relatively slow rate over a period of about 2 years.

3. Modeling and interpretation of volcano-wide deformation

We assume that the pre-eruption surface deformation was caused by a volume change beneath Kizimen due to an injection of magmatic or hydrothermal fluids. In order to explain the InSAR-derived deformation field, we first tested a point source of dilation in an elastic half-space (Mogi, 1958) that includes a correction to account for topographic variation (Williams and Wadge, 1998). We introduced linear terms in our model to account for any phase ramp due to satellite position errors (Massonnet and Feigl, 1998). We chose one descending C-band Envisat interferogram and one ascending L-band ALOS PALSAR that have the best coherence and least apparent atmospheric contaminations, and modeled them independently. Fig. 3 shows observed (a, d), modeled (b, e), and residual (c, f) interferograms. Both of the modeled interferograms fit the corresponding observed interferograms reasonably well. However, the source locations of the best fitting Mogi models are offset from each other by more than 10 km at the surface (Fig. 3b, e), and the source depths also differ considerably (6.5 km and 11.4 km below sea level (BSL), respectively). This suggests that a single Mogi source cannot fit the deformation patterns seen in both descending and ascending interferograms, and that surface displacements might have had a sizable horizontal component. Horizontal motions affect ascending and descending interferograms differently, because in one case the motion is at least partly toward the satellite and in the other it is away from the satellite (conventional interferograms are insensitive to motion parallel to the satellite track).

Considering the differences in fringe patterns portrayed in the ascending versus descending interferogram, we next tried a uniform opening dike (i.e., crack) embedded in an elastic half-space (Okada,

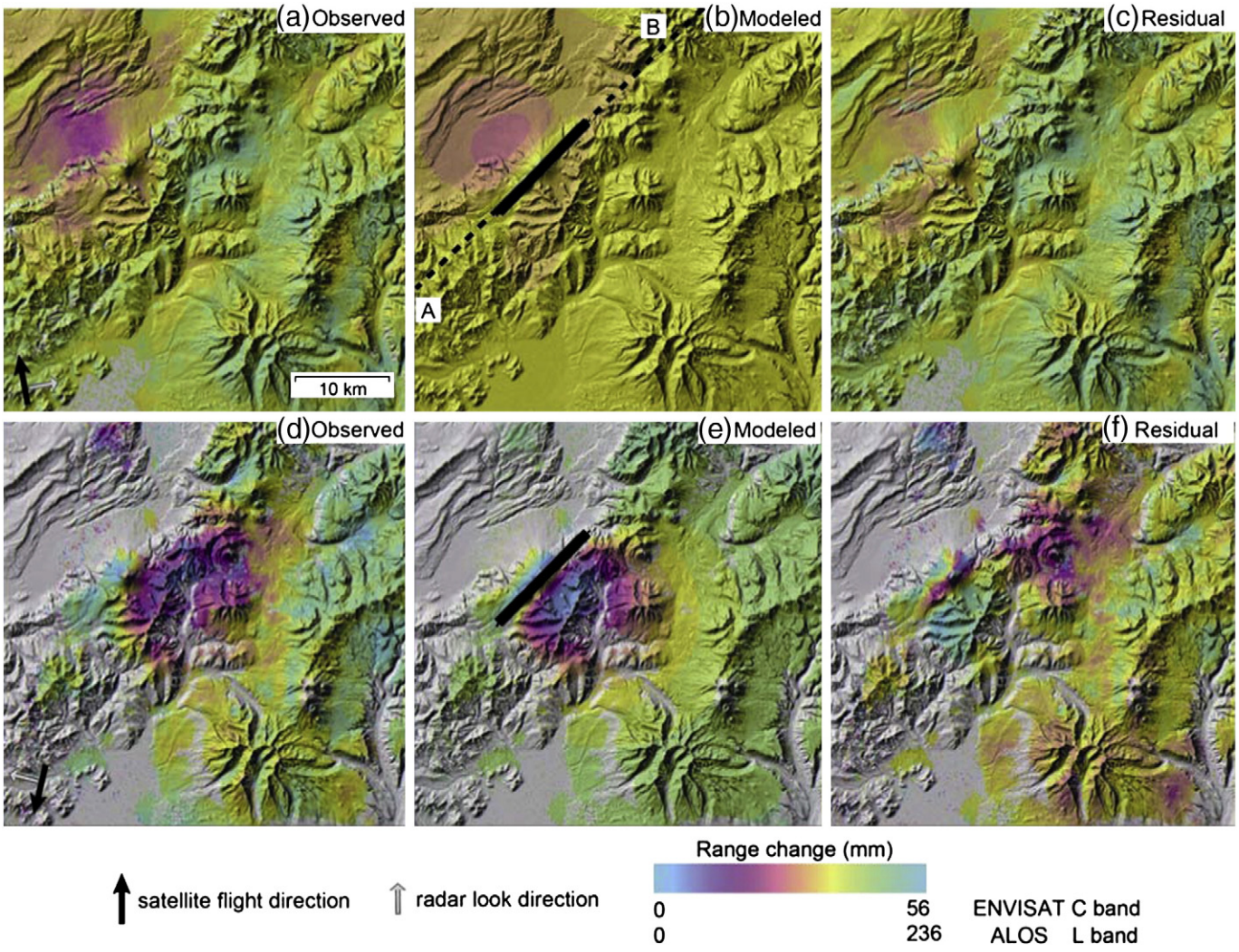

Fig. 4. (left) Observed interferograms with the best coherence spanning (a) 20070909–20100802 (ALOS PALSAR Path 358) and (d) 20090809–20100829 (ENVISAT Track 288); (middle) (b, e) synthetic interferograms for a dike model that fit both observed interferograms jointly; (right) (c, f) residual interferograms, which are the differences between observed (left) and modeled (middle) interferograms. Satellite flight direction and radar look direction are labeled on the observed interferograms. Each fringe (full color cycle) represents 56 mm or 236 mm of range change between the ground and the satellite for ENVISAT (a–c) and ALOS (d–f), respectively. Areas that lack interferometric coherence are uncolored. Thick black lines in (b) and (e) outline the projection of the best-fit dike onto the surface. The depth distribution of local earthquakes projected onto profile A–B is shown in Fig. 7.

1985) to jointly model the two interferograms (Fig. 2e, g). Eight parameters define the dike: length, width, depth, strike, dip, opening, and location (two parameters). In the model, we introduced linear terms to account for any possible phase ramp due to uncertainties in satellite positions (Massonnet and Feigl, 1998). We used the downhill simplex method and Monte Carlo simulations (Press et al., 1992) to estimate optimal parameters and their uncertainties, and the root mean square errors (RMSE) between the observed and modeled interferograms as the prediction-fit criterion. To simplify the inversion, we constrained the strike of the model dike to be approximately NE–SW. This direction is parallel to numerous normal faults in the area (Melekestsev et al., 1995; Browne et al., 2010), to the trend of the EVF and SR volcanic belts, and to an elongate pattern of seismicity in the area (see Discussion). Fig. 4 shows observed (a, d), modeled (b, e), and residual (c, f) interferograms for the dike model. The model fits both of the two observed interferograms reasonably well. The thick black line in Fig. 4b, e represents the surface projection of the dike plane. The dike was emplaced directly beneath Kizimen and is much longer than the width of the volcanic edifice. The best-fit model dike is nearly vertical, 14.4 km long, 10.6 km wide (i.e., from top to bottom), strikes N40°E, and is 12.7 km deep at the center of dike plane (Table 3). All the model parameters are well constrained according to the uncertainties shown in Table 3. We attribute the goodness of fit to the availability of both ascending and descending interferograms.

Table 3
Parameters for the best-fitting model dike. Uncertainties correspond to 95% confidence.

Length (km)	14.4 ± 0.9
Width (km)	10.6 ± 0.8
Depth (km)	12.7 ± 0.8
Strike (N°E)	40.0 (fixed)
Dip (°)	88.8 ± 0.8
Opening (cm)	21.3 ± 2.4
X coordinate (km)	17.3 ± 0.8
Y coordinate (km)	34.4 ± 0.4

Note: The reference for the horizontal coordinates (X, Y) is the southwestern corner of the maps shown in Fig. 4.

Next we investigated the temporal evolution of the source volume change from 2004 to 2010, based on 14 interferograms with relatively good coherence. Because the deformation field covers a broad area, the source parameters could not be well constrained independently from each interferogram. Instead, we fixed the geometry of the deformation source as the one obtained by jointly modeling the best ascending and descending interferograms, as discussed above. We only estimated the

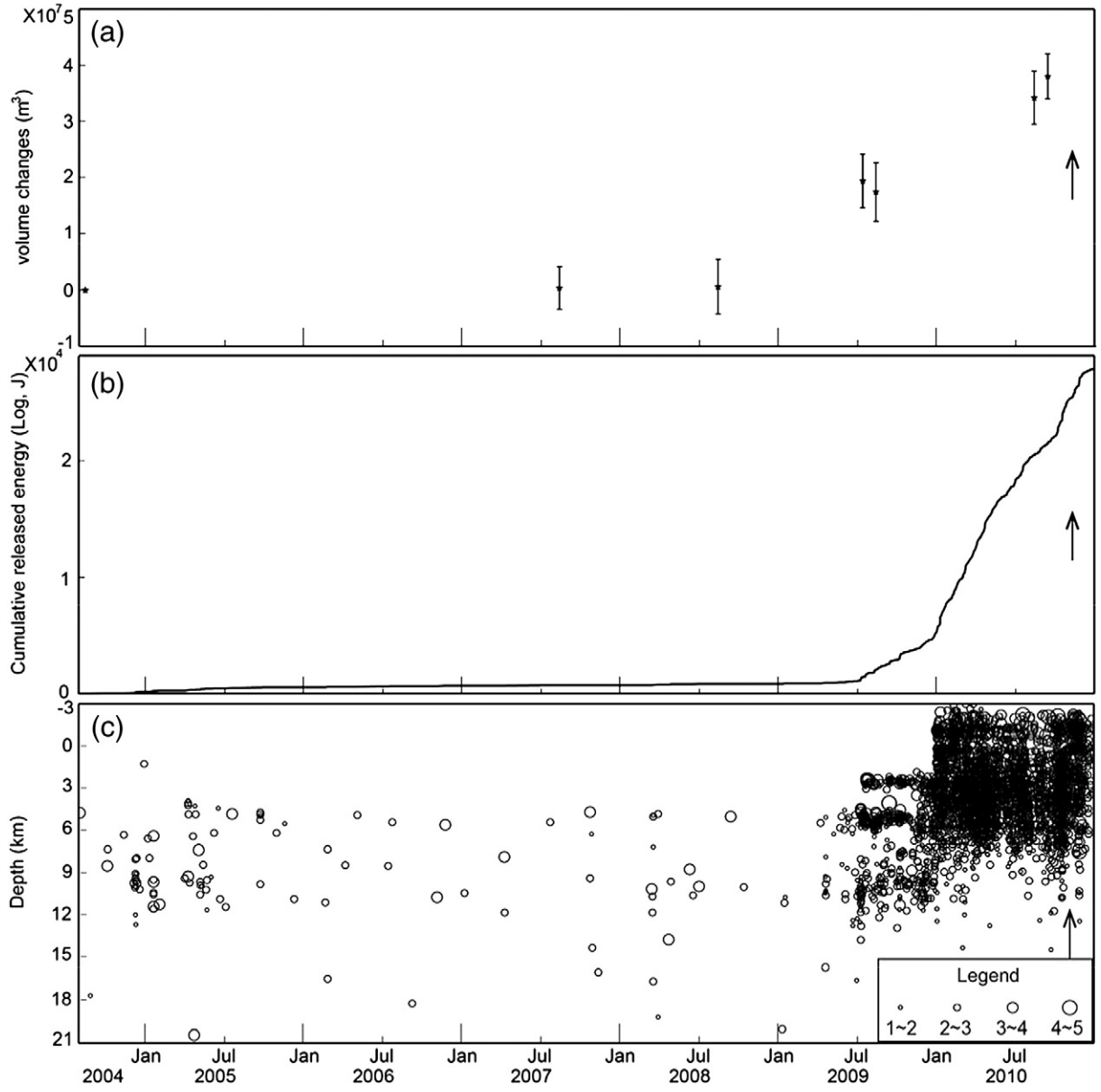

Fig. 5. (a) Estimated magma volume changes as a function of time derived from InSAR source modeling. Error bars represent one standard deviation for volume-change estimates. (b) Cumulative energy released by earthquakes from August 2004 to December 2010. (c) Distribution of hypocentral depths with time. Vertical arrows represent the eruption onset time (mid-November, 2010). Open circles in (c) denote local earthquakes; circle size is proportional to earthquake magnitude.

dike opening from the other coherent interferograms. Finally we calculated the cumulative source volume changes as a function of time. To reduce the number of time steps, SAR images that were acquired within one month of each other were assigned the same acquisition time. For example, images acquired on July 20, 2007 and August 5, 2007 were both assigned an August 2007 acquisition time. This resulted in seven image acquisition times: August 2004, August 2007, August 2008, July 2009, August 2009, August 2010 and September 2010. If we define $\mathbf{V} = (V_1, V_2, \ldots, V_i, \ldots, V_7)$, where V_i is the source volume at the ith acquisition time, then the volume changes indicated by all the interferograms, $\mathbf{L} = (L_1, L_2, \ldots, L_i, \ldots L_{14})$, is related to $\mathbf{V}$ by $\mathbf{AV^T} = \mathbf{L^T}$, where $\mathbf{A}$ is a 14 by 7 binary matrix. Unity and null elements in each row correspond to the temporal coverage for an interferogram. For instance, if the ith interferogram spans the period between the second and the third acquisition times, the second and the third columns of the ith row should be -1 and 1 corresponding to the duration of the interferogram coverage. We took the source volume corresponding to the first acquisition time (i.e. August 2004) as a reference. A weighting matrix, $\mathbf{w}$, was assembled by using the dike opening uncertainties for the diagonal elements. This assumes that source volume changes estimated from all the interferograms are uncorrelated. The weighted least squares solution (e.g., Lu et al., 2005) for $\mathbf{V}$ is:

$$\mathbf{V} = \left(\mathbf{A}^T\mathbf{PA}\right)^{-1}\mathbf{A}^T\mathbf{PL^T}. \quad (1)$$

Using Eq. (1), we estimated the source volume changes as a function of time (Fig. 5a). Based on this time-series analysis of volume changes, we concluded that the dike intrusion event began sometime between August 2008 and July 2009, more than a year before the start of the 2010 eruption. We also deduced that the magma source volume increased approximately linearly with time (i.e., intrusion rate was constant), although the poor temporal resolution of InSAR images in this area imposes considerable uncertainty to that inference. According to our analysis, the magma source volume reached to

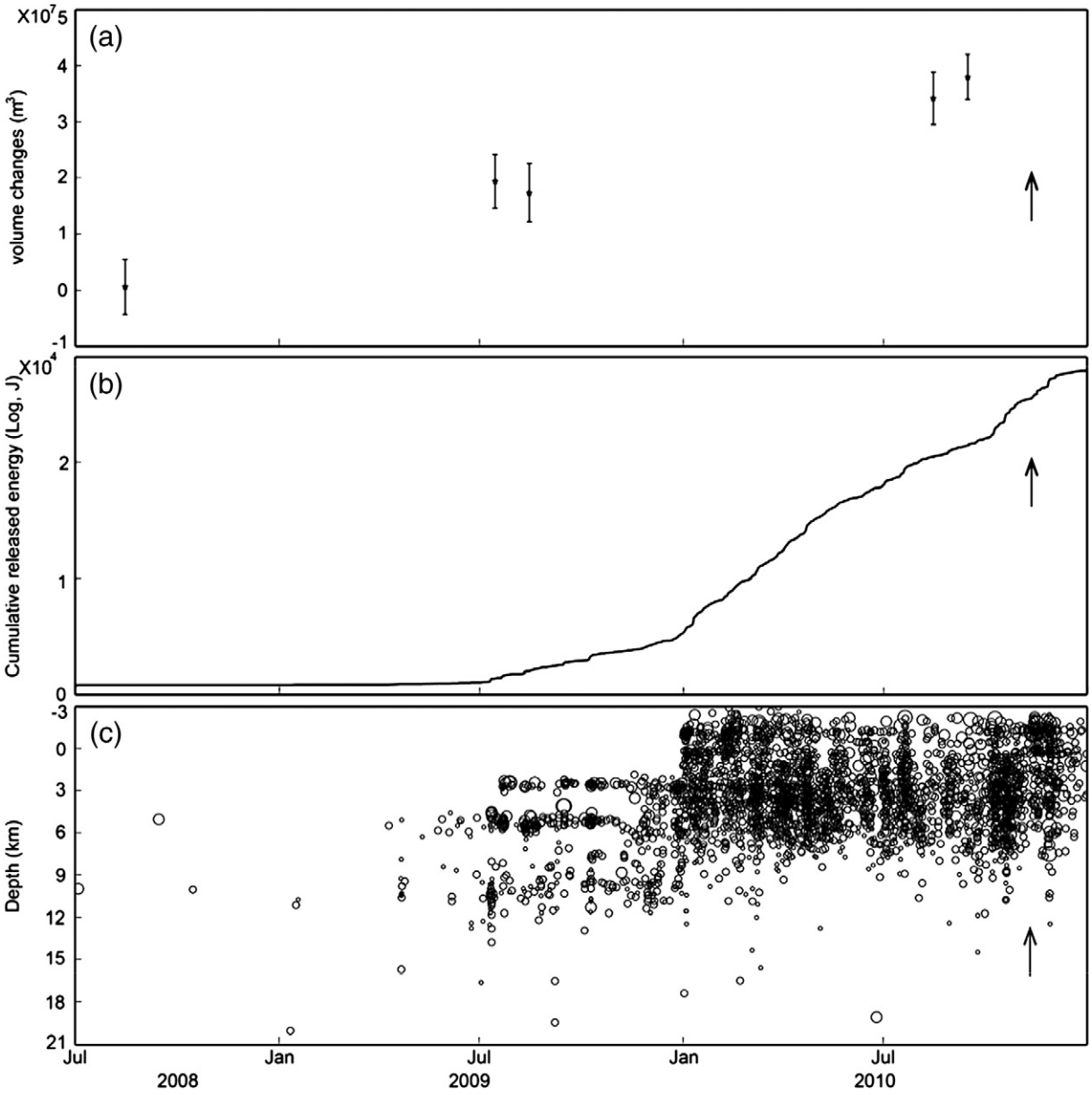

Fig. 6. Enlarged versions of the time-series plots shown in Fig. 5 for the period August 2008–December 2010. Refer to Fig. 5 caption for details.

3.2×10^7 m^3 by mid-September 2010, about two months prior to the start of the eruption in mid-November 2010.

4. Discussion

Our InSAR analysis of Kizimen volcano indicates that pre-eruption surface deformation was caused by opening of a large dike centered about 13 km beneath the edifice and extending several kilometers beyond its base to the southwest and northeast. To learn more about the intrusion, we examined the pattern of earthquakes recorded by the regional seismic network around Kizimen (Senyukov et al., 2011) (Figs. 5–7). Swarms of earthquakes with magnitudes less than 5 struck the Kizimen area starting in April 2009 (Figs. 5b–c, 6b–c), about 1.5 years before the start of the 2010 eruption. Pre-eruption earthquake swarms often are associated with magma intrusion (e.g., Lu et al., 2000; Wright et al., 2006), and sometimes delineate the propagation of an intruding dike (e.g., Einarsson and Brandsdottir, 1980). We infer that the earthquake swarms at Kizimen were caused by local stress changes due to magma intrusion. The epicentral distribution of recorded earthquakes is elongated northeastly (Fig. 7a), parallel to the strike of numerous normal faults in the area (Kozhurin et al., 2006). The number of earthquakes increased steadily with time (Figs. 5b, 6b), especially after April 2009. This is consistent with the approximately constant deformation rate we infer from our InSAR analysis. That analysis loosely constrains the onset of diking beneath Kizimen sometime between September 2008 and April 2009. Elsewhere, there is evidence that magma intrusion began several months before the occurrence of earthquake swarms (e.g., Lu et al., 2002). In other cases, the start of intrusion and increased seismicity were simultaneous (e.g., Pallister et al., 2010). If magma intrusion beneath Kizimen started around April 2009 when earthquake swarms began, the intrusion rate during April–August 2009 was about twice the rate during August 2009–September 2010. Earthquake epicenter migration is characteristic of the dike injection process (e.g., Dziak and Fox, 1999). Prior to November 2009, the earthquakes tended to cluster at one of 3 depths, ~3 km, ~6 km, and ~10 km (Figs. 5c and 6c). This was likely an artifact of the location procedure in the case of a very sparse seismic network. The depth clustering disappeared after a new seismic station was installed in November 2009. The apparent shoaling in epicenter depth starting January 2010 was due to the use of a new earthquake relocation program (Senyukov et al., 2011). However, we believe the

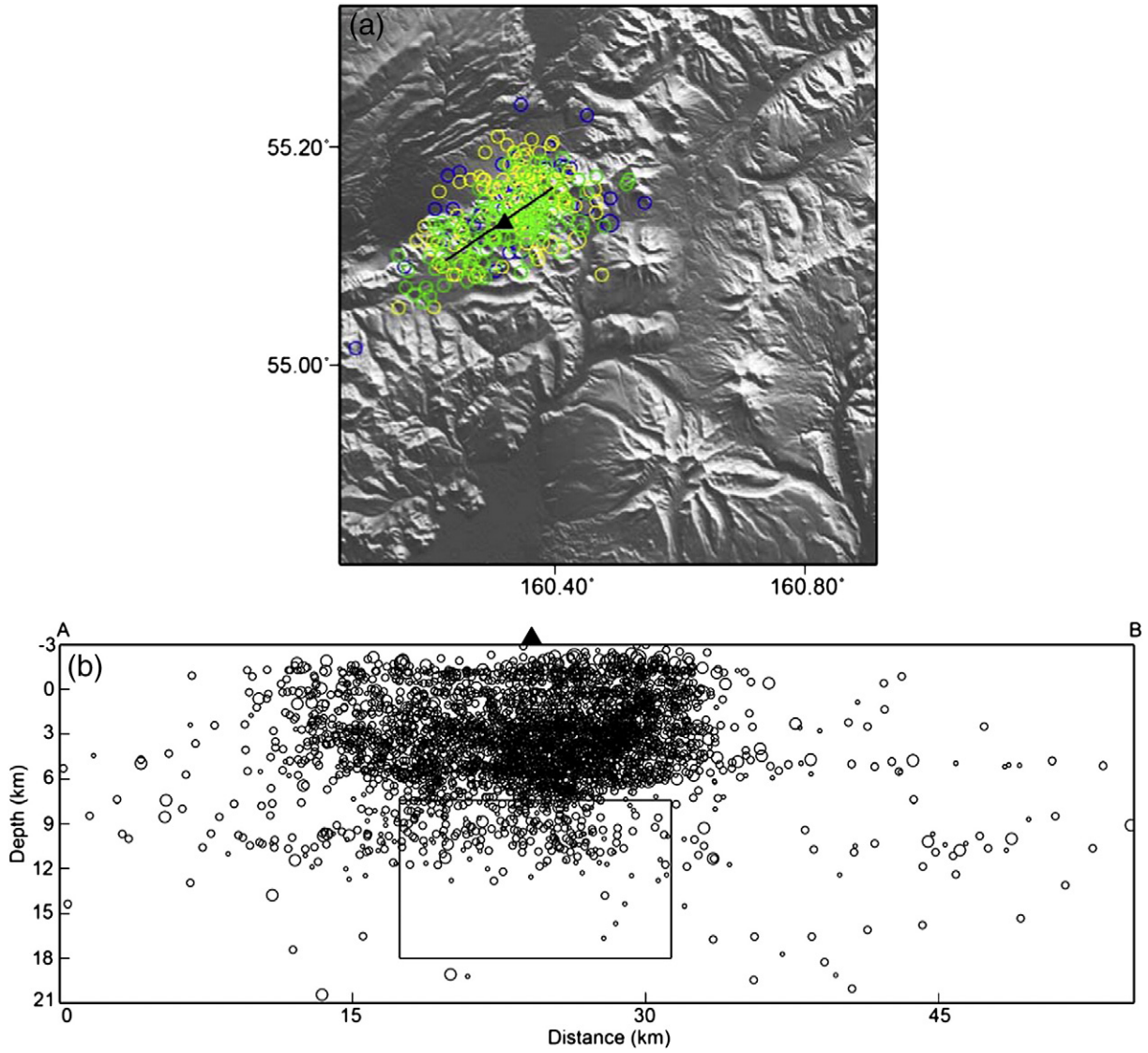

Fig. 7. (a) Epicentral distribution of earthquakes near Kizimen. Blue, yellow, and green circles represent earthquakes that occurred during July–December 2009, January–June 2010, and July 2010–November, 2011, respectively. For clarity, only earthquakes with $M_L > 3$ are shown. (b) Cross-section showing the depth distribution of earthquakes recorded from July 2009 to November 2010. Hypocenters were projected onto profile A–B (see Fig. 4b). Kizimen volcano is marked with black triangle, with surface projection of best-fit dike indicated by black line. Rectangle below shows boundaries of best-fit dike prior to its ascent to the surface. Open circles have same meaning as in Figs. 5 and 6. (For interpretation of the references to color in this figure legend, the reader is referred to the web version of this article.)

overall increase of seismic energy release starting early 2010 was real, which suggests the continuous opening of the intruded dike. The distribution of epicenters along the inferred dike trend (Fig. 7b) suggests that most of the earthquakes occurred above the tip of the dike, where strain would be greatest. Similar patterns have been observed prior to dike-fed eruptions at other volcanoes, for example, the September 1999 eruption of Kilauea volcano (Cervelli et al., 2002), July 2001 eruption of Etna volcano (Bonaccorso et al., 2002; Patane et al., 2002), and 2000–2003 eruption of Piton de La Fournaise volcano (Peltier et al., 2005).

Based on our InSAR analysis and interpretation of seismicity patterns, we conclude that dike intrusion played a major role in triggering the 2010 Kizimen eruption. We infer that magma migrated from a deep source region into a storage zone perhaps 7–18 km BSL beneath Kizimen sometime between September 2008 and April 2009. The regional stress field favors the formation of dikes rather than a spherical reservoir beneath the volcano, and as a result the intruding magma accumulated in an elongate, dike-like storage zone. The zone dilated progressively over time, accompanied by sporadic earthquakes and subtle surface deformation. Continuing intrusions caused the intruded zone to widen, causing more surface deformation and increased seismicity. Eventually, increasing magma pressure in the growing intrusion exceeded the confining strength of the host rock and magma breached the surface at the weakest part of the system, triggering the mid-November 2010 eruption at Kizimen.

5. Conclusions

By combining both C-band ENVISAT and L-band ALOS InSAR images, we mapped a broad pattern of surface deformation that occurred at Kizimen volcano during 2008–10 and culminated in an explosive eruption starting in mid-November 2010. Deformation modeling suggests that emplacement of a near-vertical dike striking approximately NE–SW was responsible for the observed pre-eruption deformation. The intrusion began sometime after August 2008, likely around April 2009 when local seismicity increased dramatically. The intrusion volume increased at a roughly constant rate through September 2010. In mid-November 2010, increasing magma pressure in the dike exceeded the confining strength of the host rock and the 2010 eruption ensued.

InSAR observations from this study provide a glimpse of large scale pre-eruption deformation associated with a major diking event. There

is no ground-based deformation monitoring network at Kizimen, so if not for InSAR observations we would know little about the event. Thus InSAR can provide important insights into magma storage and transport processes, especially at volcanoes that are poorly monitored owing to their remoteness, difficult logistics, or other factors.

Acknowledgments

The first author would like to thank the China Scholarship Council for funding a one-year InSAR study at the Cascades Volcano Observatory, U.S. Geological Survey (USGS). This research was supported by the USGS Volcano Hazards Program, USGS Volcano Science Center, NASA grant 11-DESSDT11-0021, and Natural Science Foundation of Shanxi, China (No. 2011021024-1). ENVISAT SAR data are copyrighted by ESA and were provided by ESA under CAT1-2765. ALOS SAR data are copyrighted by JAXA/METI and were provided by the Alaska Satellite Facility (ASF) and JAXA.

References

Amelung, F., Jonsson, S., Zebker, H., Segall, P., 2000. Widespread uplift and 'trapdoor' faulting on Galapagos volcanoes observed with radar interferometry. Nature 407, 993–996.

Biggs, J., Anthony, E.Y., Ebinger, C.J., 2010. Multiple inflation and deflation events at Kenyan volcanoes, East African Rift. Geology 37, 979–982. http://dx.doi.org/10.1130/G30133A.1.

Bonaccorso, A., Aloisi, M., Mattia, M., 2002. Dike emplacement forerunning the Etna July 2001 eruption modeled through continuous tilt and GPS data. Geophysical Research Letters 29 (13), 1624. http://dx.doi.org/10.1029/2001GL014397.

Browne, B., Izbekov, P., Eichelberger, J., Churikova, T., 2010. Pre-eruptive storage conditions of the Holocene dacite erupted from Kizimen Volcano, Kamchatka. International Geology Review 52 (1), 95–110.

Calais, E., d'Oreye, N., Albaric, J., Deschamps, A., Delvaux, D., Deverchere, J., Ebinger, C., Ferdinand, R.W., Kervyn, F., Macheyeki, A.S., Oyen, A., Perrot, J., Saria, E., Smets, B., Stamps, D.S., Wauthier, C., 2008. Strain accommodation by slow slip and dyking in a youthful continental rift, East Africa. Nature 456. http://dx.doi.org/10.1038/nature07478.

Cervelli, P., Segall, P., Amelung, F., Garbeil, H., Meertens, C., Owen, S., Miklius, A., Lisowski, M., 2002. The 12 September 1999 Upper East Rift Zone dike intrusion at Kilauea Volcano, Hawaii. Journal of Geophysical Research 107 (B7). http://dx.doi.org/10.1029/2001JB000602.

Dvorak, J.J., Dzurisin, D., 1997. Volcano geodesy: the search for magma reservoirs and the formation of eruptive vents. Reviews of Geophysics 35 (3), 343–384.

Dziak, R.P., Fox, C.G., 1999. The January 1998 Earthquake swarm at Axial Volcano, Juan de Fuca Ridge: Hydroacoustic evidence of seafloor volcanic activity. Geophysical Research Letters 26 (23), 3429–3432. http://dx.doi.org/10.1029/1999GL002332.

Dzurisin, D., 2007. Volcano Deformation — Geodetic Monitoring Techniques. Springer-Praxis Publishing Ltd., Chichester, UK.

Einarsson, P., Brandsdottir, B., 1980. Seismological evidence for lateral magma intrusion during the July 1978 deflation of the Krafla volcano in NE-Iceland. Journal of Geophysics 47, 160–165.

Farr, T.G., Rosen, P.A., Caro, E., Crippen, R., Duren, R., Hensley, S., Kobrick, M., Paller, M., Rodriguez, E., Roth, L., Seal, D., Shaffer, S., Shimada, J., Umland, J., Werner, M., Oskin, M., Burbank, D., Alsdorf, D., 2007. The shuttle radar topography mission. Reviews of Geophysics 45 (2), RG2004.

Kozhurin, A.I., 2004. Active faulting at the Eurasian, North American and Pacific plates junction. Tectonophysics 380 (3–4), 273–285. http://dx.doi.org/10.1016/j.tecto.2003.09.024.

Kozhurin, A., Acocella, V., Kyle, P.R., Lagmay, F.M., Melekestsev, I.V., Ponomareva, V., Rust, D., Tibaldi, A., Tunesi, A., Corazzato, C., Rovida, A., Sakharov, A., Tengonciang, A., Uy, H., 2006. Trenching active faults in Kamchatka, Russia: paleoseismological and tectonic implications. Tectonophysics 417, 285–304.

Lu, Z., 2007. InSAR imaging of volcanic deformation over cloud-prone areas — Aleutian islands. Photogrammetric Engineering and Remote Sensing 73 (3), 245–257.

Lu, Z., Mann, D., Freymueller, J., Meyer, D., 2000. Synthetic aperture radar interferometry of Okmok volcano, Alaska: radar observations. Journal of Geophysical Research 105 (10), 10,791–10,806.

Lu, Z., Wicks, C., Dzurisin, D., Power, J., Moran, S., Thatcher, W., 2002. Magmatic inflation at a dormant stratovolcano: 1996–98 activity at Mount Peulik volcano, Alaska, revealed by satellite radar interferometry. Journal of Geophysical Research 107 (B7), 2134. http://dx.doi.org/10.1029/2001JB000471.

Lu, Z., Masterlark, T., Dzurisin, D., 2005. Interferometric synthetic aperture radar study of Okmok volcano, Alaska, 1992–2003: magma supply dynamics and postemplacement lava flow deformation. Journal of Geophysical Research 110, B02403. http://dx.doi.org/10.1029/2004JB003148.

Lu, Z., Dzurisin, D., Biggs, J., Wicks, J.C., McNutt, S., 2010. Ground surface deformation patterns, magma supply, and magma storage at Okmok volcano, Alaska, from InSAR analysis: 1. Intereruption deformation, 1997–2008. Journal of Geophysical Research 115, B00B02. http://dx.doi.org/10.1029/2009JB006969.

Lundgren, P., Lu, Z., 2006. Inflation model of Uzon caldera, Kamchatka, constrained by satellite radar interferometry observations. Geophysical Research Letters 33, L06301. http://dx.doi.org/10.1029/2005GL025181.

Massonnet, D., Feigl, K., 1998. Radar interferometry and its application to changes in the Earth's surface. Reviews of Geophysics 36, 441–500.

Massonnet, D., Briole, P., Arnaud, A., 1995. Deflation of Mount Etna monitored by spaceborne radar interferometry. Nature 375, 567–570.

Melekestsev, I.V., Ponomareva, V.V., Volynets, O.N., 1995. Kizimen Volcano, Kamchatka — a future Mount St. Helens? Journal of Volcanology and Geothermal Research 65, 205–226.

Melnikov, D.V., Dvigalo, V.N., Melekestsev, I.V., 2011. The 2010–2011 eruption of Kizimen volcano, Kamchatka: dynamics of eruptive activity and geologic-geomorphological impact (based on remote sensing data). Bulletin of Kamchatka Association "Educational-Scientific Center". Earth Sciences 2 (18), 87–101 (in Russian).

Mogi, K., 1958. Relations between the eruptions of various volcanoes and the deformations of the ground surface around them. Bulletin. Earthquake Research Institute, University of Tokyo 36, 99–134.

Okada, Y., 1985. Surface deformation due to shear and tensile faults in a half-space. Bulletin. Seismological Society of America 75, 1135–1154.

Pallister, J., McCausland, W., Jónsson, S., Lu, Z., Zahran, H., Hadidy, S., Aburukbah, A., Stewart, I., Lundgren, P., White, R., Moufti, M., 2010. Broad accommodation of rift-related extension recorded by dyke intrusion in Saudi Arabia. Nature Geoscience 3, 705–712.

Patane, D., Chiarabba, C., Cocina, O., Gori, P.D., Moretti, M., Boschi, E., 2002. Tomographic images and 3D earthquake locations of the seismic swarm preceding the 2001 Mt. Etna eruption: Evidence for a dyke intrusion. Geophysical Research Letters 29 (10), 1497. http://dx.doi.org/10.1029/2001GL014391.

Peltier, A., Ferrazzini, V., Staudacher, T., Bachèlery, P., 2005. Imaging the dynamics of dyke propagation prior to the 2000–2003 flank eruptions at Piton de La Fournaise, Reunion Island. Geophysical Research Letters 32, L22302. http://dx.doi.org/10.1029/2005GL023720.

Ponomareva, V., Melekestsev, I., Braitseva, O., Churikova, T., Pevzner, M., Sulerzhitsky, L., 2007. Late Pleistocene–Holocene volcanism on the Kamchatka Peninsula, northwest Pacific region. In: Eichelberger, J., Gordeev, E., Izbekov, P., Kasahara, M., Lees, J. (Eds.), Volcanism and Subduction: The Kamchatka Region: Amer Geophys Union, Geophys Monogr., 172, pp. 165–198.

Press, W., Teukolsky, S., Vetterling, W., Flannery, B., 1992. Numerical Recipes in C, the Art of Scientific Computing. Cambridge Univ. Press, New York, p. 994.

Pritchard, M.E., Simons, M., 2004. Surveying volcanic arcs with satellite radar interferometry: the central Andes, Kamchatka, and beyond. GSA Today 14 (8), 4–11.

Rosen, P.A., Hensley, S., Zebker, H., Webb, F.H., Fielding, E.J., 1996. Surface deformation and coherence measurements of Kilauea Volcano, Hawaii, from SIR-C radar interferometry. Journal of Geophysical Research 101, 23,109–23,125.

Rosen, P.A., Hensley, S., Joughin, I.R., Li, F.K., Madsen, S.N., Rodriguez, E., Goldstein, R.M., 2000. Synthetic aperture radar interferometry. Proceedings of the IEEE 88, 333–380.

Senyukov, S.L., Nuzhdina, I.N., Droznina, S.J., Garbuzova, V.T., Kozhevnikova, T.Y., Sobolevskaya, O.V., 2011. Seismicity of the volcano Kizimen. Proceedings of the 3 conference "Problems of geophysical monitoring of Far East of Russia", Petropavlovsk-Kamchatsky, Russia, 09–15 October 2011, pp. 144–148 (in Russian).

Siebert, L., Simkin, T., 2002. Volcanoes of the world: an illustrated catalog of Holocene volcanoes and their eruptions. Smithsonian Institution, Global Volcanism Program Digital Information Series, GVP-3.

VONA/KVERT, 2012. Information Release. December 27 KVERT, Institute of Volcanology and Seismology FEB RAS (URL: http://www.kscnet.ru/ivs/kvert/van/index.php?n=2012-25).

Williams, C.A., Wadge, G., 1998. The effects of topography on magma chamber deformation models: application to Mt. Etna and radar interferometry. Geophysical Research Letters 25, 1549–1552.

Wright, T.J., Ebinger, C., Biggs, J., Ayele, A., Yirgu, G., Keir, D., Stork, A., 2006. Magma-maintained rift segmentation at continental rupture in the 2005 Afar dyking episode. Nature 442, 291–294.

Yun, S., Segall, P., Zebker, H., 2006. Constraints on magma chamber geometry at Sierra Negra Volcano, Galapagos Islands, based on InSAR observations. Journal of Volcanology and Geothermal Research 150 (1–3), 232–243.